Journal of Hydrology xxx (xxxx) xxxx

Contents lists available at ScienceDirect

Journal of Hydrology

journal homepage: www.elsevier.com/locate/jhydrol

Research papers

A new distributed karst-tunnel hydrological model and tunnel hydrological effect simulations

Ji Li[a], Aihua Hong[b], Daoxian Yuan[a,c], Yongjun Jiang[a,*], Shujin Deng[b], Cong Cao[b], Jiao Liu[d]

[a] Chongqing Key Laboratory of Karst Environment & School of Geographical Sciences of Southwest University, Chongqing 400715, China
[b] Laboratory of Chongqing Groundwater Resourse Utilization and Environmental Protection (Nanjiang Hydrogeological Team Under the Chongqing Geological Bureau of Geology and Minerals Exploration), Chongqing 401121, China
[c] Karst Dynamic Laboratory, Ministry of Land and Resources, Guilin 541004, China
[d] Chongqing Hydrology and Water Resources Bureau, Chongqing 401120, China

ARTICLE INFO

Keywords:
Karst tunnel hydrological model (KTHM)
Hydrological effects of tunnel excavation
Tunnel submodule
Runoff simulations
Southwest China

ABSTRACT

Tunnel excavation in karst areas could affect natural karst hydrological processes and runoff, resulting in groundwater drainage and even underground river cut-off. The hydrological model is a good tool with which to study the hydrological effect of tunnels. The application of current hydrological models in karst areas usually requires a large amount of modelling data, especially hydrogeological data that are much more difficult to obtain than those in non-karst areas. To overcome the difficulty of modelling in karst areas, this study presents a new fully physically based distributed karst tunnel hydrological model (KTHM) with a simple structure and simple parameters. The underground confluence module is divided into only two layers: confluence in the epikarst zone and the underground river. Such a simple structure makes it possible to build a model in karst basins with only a small amount of hydrogeological data. In the structure of this KTHM, the tunnel is incorporated in a specially designed submodule to quantify the influence of the tunnel hydrological effect on the water volume. If the tunnel submodule is turned off, then this model becomes a karst hydrological model (KHM) and can be used in other karst basins without tunnels. The simulation results of 20 flow processes and 2 annual runoffs modelled by the KHM and KTHM are compared; the KTHM is more accurate in the study area, which indicates that the tunnel submodule in the model is necessary and that the KTHM is feasible for performing runoff simulations in the study area. The sensitivity sequence of hydrological effects of tunnels on runoff in karst areas is as follows: dry season runoff volume > normal runoff volume > interannual runoff volume > flood peak flow > flood volume.

1. Introduction

Tunnel excavation in karst areas will affect the local karst water system, which is mainly reflected in changes in the groundwater flow field, the water cycle processes, rules, and ultimately the spatial and temporal distribution patterns of karst water resources (Yuan, 2002; Hartmann et al., 2014). Because the hydrogeological conditions in karst areas are more complicated and changeable than those in non-karst areas, tunnel excavation in karst areas is more likely to affect more fragile and sensitive karst water systems, thereby leading to interruptions of the natural hydrological cycle or problems in the ecological environment, such as surface water leakage, karst water inrush, groundwater drainage, and karst collapse (Iacobellis et al., 2015; Vigna et al., 2017).

Tunnels are densely distributed in the Zhongliangshan karst valley basin in Chongqing, China, the study area of this paper. There are three tunnels within a range of only 12 km^2, with an average spacing of approximately 2 km. Several more tunnels are planned to be built. This phenomenon of densely packed tunnels is common in mountain cities such as Chongqing. In the study area, according to a previous basin survey, these tunnels have had serious impacts on the local karst water system and ecological environment (Lv et al., 2020). The underground river in the study area previously flowed regularly but is now occasionally cut off under the influence of the tunnels, and a large area of former paddy fields has become dry land. There were fifteen epikarst springs in the basin before 2000, which are the main source of water supply for local residents' livelihood and irrigation needs. However, only one spring with low discharge was found in 2017 (Liu et al., 2019), and it is now often cut off during the dry season. Therefore, studying the hydrological effects of tunnel excavation in the study area is necessary.

In this study, we focus on the impact of tunnel engineering on the

* Corresponding author.
E-mail address: jiangjyj@swu.edu.cn (Y. Jiang).

https://doi.org/10.1016/j.jhydrol.2020.125639

Available online 14 October 2020
0022-1694/ © 2020 Elsevier B.V. All rights reserved.

runoff process and water quantity at natural underground river outlets in the study area, where there are no surface rivers, and an underground river within the basin is the only confluence of drainage. After a tunnel was built, it drained some of the water that should have flowed from the underground river. The water volume at the underground river outlet should be reduced; however, the expected level of reduction was not clear. Although a gauging station has been set up at the underground river outlet, it was installed after completion of a tunnel, and the changes in underground runoff before and after tunnel construction cannot be compared. Therefore, it is necessary to establish a mathematical-physical model to quantitatively compare the impact of tunnel engineering on natural runoff in karst areas, and hydrological models can represent good tools for such investigations (Goldscheider and Drew, 2007; Li et al., 2019a, 2019b).

Recent research on the hydrological modelling in karst basins with tunnels has focused on mainly the prediction of tunnel water inrush (Linbin et al., 2010; Wang et al., 2019; Neukomm et al., 2020), for which MODFLOW, for example, is widely used (Reimann et al., 2009; Gallegos et al., 2013), simulations of underground water flow regimes or seepage fields under the influence of tunnels (Raposo et al., 2010; Chen et al., 2020), engineering geological hazards caused by tunnel construction, such as karst collapse (Zini et al., 2015; Lv et al., 2020), and the environmental impacts of tunnelling in karst regions (Milanovic, 2002; Bonacci, 2014; Parise et al., 2015; Liu et al., 2019). In addition, some classic hydrological models, such as the SHE model (Abbott et al., 986a; Abbott et al., 1986b), SWAT model (Peterson and Hamlett,1998), and TOPMODEL (Ambroise et al., 1996), are often used in hydrological simulations and predictions in karst areas (Doummar et al., 2012; Li et al., 2012; Ren, 2016; Baffaut and Benson, 2009; Suo et al., 2007; Pan, 2014).

Although the above simulations and predictions by hydrological models have achieved good research results in karst basins with tunnels, the cost of modelling in karst areas is relatively high. On the one hand, the intricate underlying surface conditions and hydrogeological characteristics in karst areas pose great challenges for accurately simulating hydrological effects of tunnels (Fiorillo et al., 2015; Xu et al., 2020). In particular, the anisotropic interactions of karst aquifers make it difficult to accurately describe the movement and transformation of rainfall infiltration water in karst water-bearing media (Milanovic, 2002; Bartolomé et al., 2006). On the other hand, hydrological models, especially distributed hydrological models (Freeze and Harlan, 1969), usually have multiple and complex structures with many parameters (Chen, 2009, 2018; Hartmann et al., 2015), so more data, especially a large amount of hydrogeological data, are needed to build the model. In addition, obtaining these data is much more difficult in karst areas than in non-karst areas (Ford and Williams, 2007; Vincenzi et al., 2009). For example, borehole pumping tests are needed to determine the influence of tunnel construction on karst groundwater dynamics (Birk et al., 2005; Schiller and Renard, 2016).

To address the difficulty of insufficient data for distributed models used in karst areas, in this study, a new fully distributed karst tunnel hydrological model (KTHM) is developed to simulate hydrological effects of tunnels in detail. Unlike other distributed hydrological models used in karst basins, which often require a considerable amount of data to build the model due to their complex structural features (Kraller et al., 2014; Hartmann et al., 2015), this new KTHM has particular advantages when used in karst areas. The model structure is relatively simple, and its overall structure is divided into only two parts: the surface and the underground parts. The main function of the former is to converge surface rivers into the underground river system, while the latter corresponds to the confluent output of the karst underground river in the basin. Therefore, this KTHM is an integration of a surface hydrological model and groundwater flow model in terms of its mechanism. The underground confluence module of the vertical structure is also divided into two layers, and the physical significance of each layer is explicit and simple, which makes it possible to build models that represent karst areas with only limited meteorological and hydrogeological data. In addition, the model is calibrated and validated against field hydrogeological data that can be easily obtained by, for example, tracer experiments. The model parameters are classified and dimensionless, and only the moderate and high-sensitivity parameters need to be optimized, which saves calculation time. This new KTHM has great potential for application in karst areas due to these advantages.

In the model structure of the KTHM, a tunnel submodule is designed as an independent structure for detailed simulations of the response of hydrological processes to tunnels in the study area. In the tunnel submodule, considering that the shape of the tunnel is usually regular, the water movement in the tunnel basically conforms to Darcy's law, and parameters such as the distribution, shape and size of the tunnel are easy to obtain. Thus, this study refers to the algorithm of MODFLOW-CFPM1 (Gallegos et al., 2013) for tunnel drainage simulations. In addition, to describe runoff generation and confluence in anisotropic water-bearing karst media, karst aquifers need to be discretized effectively. This discrete method in the KTHM is revised from the MODLOW-CFPM1 module (Qin and Jiang, 2014). When the tunnel submodule is turned off, the model becomes a karst hydrological model (KHM). The simulated water quantity difference between the KHM and the KTHM can reflect the influence of tunnels on the flow processes and runoff quantity in the study area, and 20 flow processes and 2 annual runoffs of the underground river outlet are selected to verify the performance of the KTHM in karst simulations.

2. Study area and data

2.1. Study area

The Zhongliangshan karst basin in Chongqing, a highly developed karst area in Southwest China, is selected as the study area. It is located at 106°23′E–106°28′E, 29°41′N–29°48′N. The basin area is approximately 12 km^2, and karst trough valley is the main landform. The average annual temperature is 18.3 °C, and the subtropical monsoon climate brings abundant rainfall to the basin. The average annual precipitation is 1100 mm (Liu et al., 2019), which is mainly concentrated in the flood season from April to October.

The terrain of the basin consists of three low mountains with two karst trough valleys, and the elevations of the mountains range from 200 to 700 m. The main exposed strata form the Guanyinxia anticline, where the core of the anticline is a karst aquifer composed of limestone and the strata are the Lower Triassic Feixianguan Formation (T_1f). The formations on both sides of the anticline core are the middle series of the Leikoupo Formation (T_2l) and the lower series of the Jialing River Formation (T_1J). The formation at the two sides of the basin is the Upper Triassic Xujiahe Formation (T3xj) and Lower Jurassic Pearl Chong Formation (J1z), where the lithologies are feldspar-quartz sandstone, shale and mudstone (Wu et al., 2018). Fig. 1 shows the Zhongliangshan karst basin map.

There are currently three tunnels in the study area, and their basic information is shown in Table 1.

2.2. Data preparation

The basic data for building the distributed hydrological model are mainly digital elevation model (DEM) data, soil type data and land use data; among them, the high-resolution DEM data are the key to dividing the karst subwatershed. The original DEM data, soil type data and land use data can be freely downloaded from databases at official websites (site links are provided later in this article); the spatial resolution of the DEM is 30 m × 30 m, while the resolutions for the soil type and land use data are 1000 m × 1000 m. These are low resolutions for such a small study area (12 km^2). According to the research results of the correlation between the area of the karst watershed and the spatial

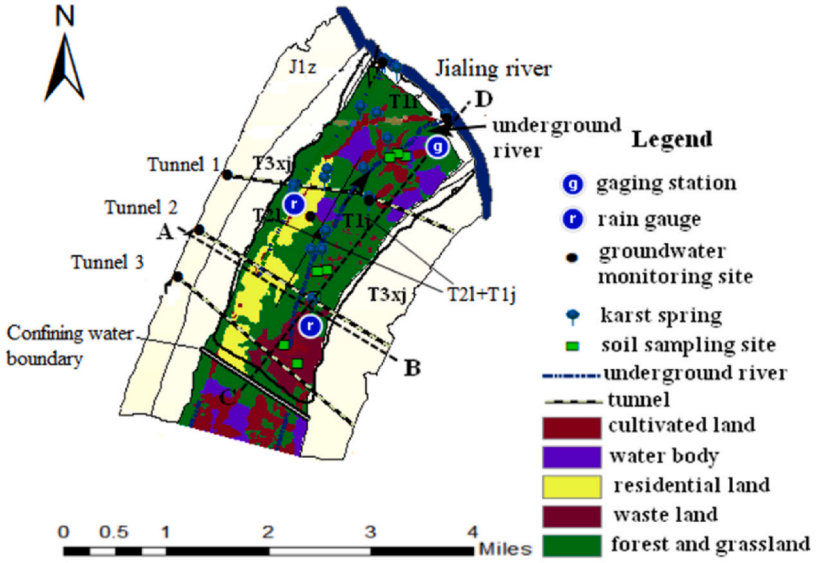

a. Land use pattern and sampling point distribution (modified from Wu et al.,2018)

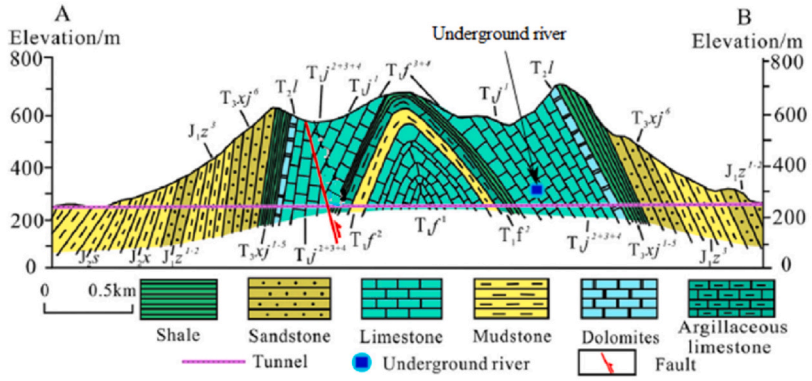

b. Lithologic map of the tunnel cross-section (modified from Liu et al.,2019)

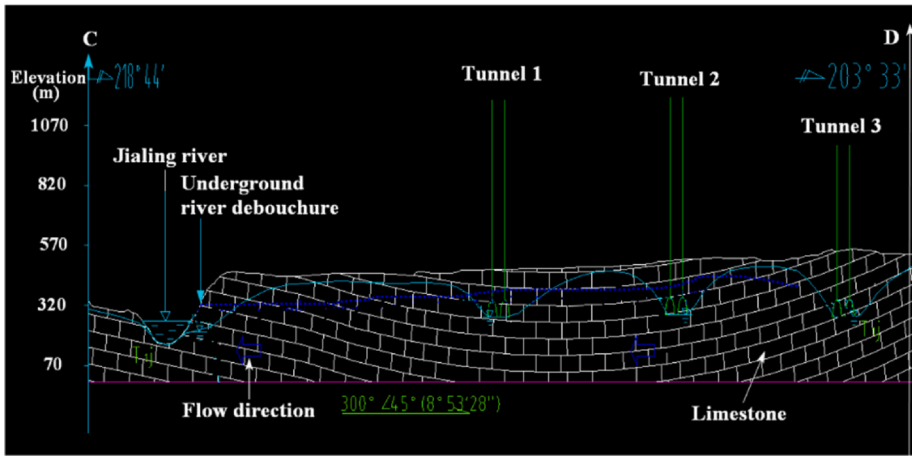

c. Longitudinal section plan of CD

Fig. 1. Zhongliangshan karst valley watershed.

resolution of the distributed model (Chen et al.,2017), the spatial resolutions of the DEM, soil type and land use data are resampled at 15 m × 15 m for the KTHM using ArcGIS 10.2 software.

Rainfall is the main recharge source of karst underground water in the basin, and the outlet discharge of the underground river responds quickly to rainfall, for which the response time of the peak discharge is 6–8 h. The tracer experiment results in the study area show that the boundary between the surface watershed and the subsurface river confluence is basically consistent and that water supply replenishment does not occur from adjacent watersheds. A direct hydraulic connection is observed between tunnel drainage and the underground river. The karst morphology of the underground river is extremely developed, which is manifested as a large single karst conduit without obvious water system branches. There may be subterranean pools or lakes along

ARTICLE IN PRESS

Table 1
Information on the three tunnels in the study area.

Tunnel No.	Tunnel Names	Build period	East/west elevation (m)	Tunnel length (km)	Tunnels under-crossing stratum
1	Shijiangliang tunnel of Chongqing Ring Highway	2006–2008	260/245	4.285	East: T_3xj, T1j, T2l West: J_1z, T_3xj, T_1f
2	Beibei tunnel of Yuwu Expressway	1999–2001	250/240	4.035	East: T_3xj, T1j, T_2l West: J1z, T_3xj, T1f
3	Beibei district Metro Line 6	2010–2013	245/240	4.322	East: T3xj, T1j, T2l West: J1z, T2l, T1f

the underground rivers; they are embodied in the KTHM as underground reservoir cells, and their storage capacity can be estimated based on tracer recovery and retention time. Then, the number of reservoir cells can be deduced by setting their water storage in the model.

The land use types in the study area are mainly cultivated land, forest and grassland, barren karst waste land, and residential land. There are three soil types: zonal yellow soil, unsaturated Cambisol, and chromic Luvisol, which account for 53%, 38.5%, and 8.5% of the basin area, respectively (Liu et al., 2019).

In this study area, 20 flows and 2 annual runoffs of the underground river outlet are selected to verify the performance of the KTHM in karst simulations. To describe the hydrological effects of tunnelling on the karst hydrological processes within a year in detail, the 20 flow processes are divided into flood runoff, dry season runoff, and normal runoff. Flood runoff refers to a peak discharge greater than 500 L s^{-1} and total flood greater than 160,000 L; dry season runoff refers to a peak discharge less than 200 L s^{-1} and total flood less than 80,000 L; and normal runoff corresponds to conditions between these limits.

3. Development and validation of the KTHM

3.1. Model development

In this study, a new distributed KTHM is developed to simulate the hydrological effects of tunnels in detail. The structure of the KTHM is explicit and has physical significance. The vertical structure is divided into two parts: the surface and the underground parts. The surface part controls the recharge from surface rivers to the underground river system, and the underground part corresponds to the confluent output of the karst underground river.

The runoff generation and confluence modes change in different karst landforms; thus, in the KTHM, the rainfall runoff is calculated by the excess infiltration runoff in exposed karst landform units and by the runoff yield under saturated storage in buried karst landforms. In the vertical model structure, five layers are created: vegetation cover, soil layer, rock strata of the epikarst zone, bedrock, and the underground river system, from top to bottom. The underground confluence module in the model is divided into only two layers: The epikarst zone and the underground river. Such a simple model structure makes it possible to build a model in karst areas with only a small amount of hydrogeological data. The horizontal structure includes river cells, hill slope cells, and reservoir cells. Fig. 2 shows the modelling and calculation flow chart of the KTHM.

3.1.1. Tunnel submodule

The tunnel submodule is an independent structure in the KTHM and is used to simulate the decrease in water volume at the underground river outlet under the influence of the tunnel in the study area. In the tunnel submodule, some simplification is needed to calculate the rainfall-runoff and confluence processes within the tunnels, which can be generalized into many large multisection circular pipelines due to their shape and structural characteristics. Considering that tunnel engineering in karst areas is usually performed in the unsaturated zone, water movement in regularly shaped pipelines basically conforms to Darcy's law. When the water surface in the pipe rises or falls, the change in flow into the unfilled pipelines can be calculated based on the MODFLOW-CFPM1 module by the following formula (Valiantzas, 2008; Qin and Jiang, 2014):

$$\begin{cases} Q_{\Delta t} = \frac{V_{t1} - V_{t0}}{\Delta t} \\ V_t = \frac{(\theta_t - \sin(\theta_t))d^2 \Delta l \tau}{8} \end{cases} \quad (1)$$

where

$$\theta = 2\sin^{-1}\left(\frac{2\sqrt{D(d-D)}}{d}\right) \quad (2)$$

where $Q_{\Delta t}$ is the flow difference between the inflow and outflow rates per unit area in the unfilled pipes, L s^{-1}; $V_{t1} - V_{t0}$ is the change in water volume during period Δt, L; V_t is the amount of water in the pipe at time t, L; θ is the angle between the water level in the pipe and the pipe radius, °; d and D are the pipe radius and diameter, dm; Δl is the length of the pipeline, dm; and τ is the pipe tortuosity.

In the tunnel submodule of the KTHM, water is exchanged between each pipe node and the adjacent fissure grid node, which can be determined by the following equation (Meseguer and Mellibovsky, 2007):

$$Q_{ex} = \sum_{jp=1}^{np} \frac{(K_w)_{ijk} \pi d_{jp} \frac{1}{2}(\Delta l_{jp} \tau_{jp})}{r_{jp}} (h_n - h_{ijk}) \quad (3)$$

where $Q_{ex}$is the water exchange in the tunnel submodule, L s^{-1}; h_{ijk} and h_n are the water heads of the ijkth grid and the adjacent nth pipe node, respectively, dm; K_w is the pipeline permeability coefficient, dm d^{-1}; r_{jp} and d_{jp} are the radius and diameter of the jpth pipeline, respectively, dm; Δl_{jp} is the length between the jth and pth pipelines, dm; and τ_{jp} is the pipe tortuosity.

3.1.2. Rainfall interpolation and evapotranspiration calculation

A limited number of rain gauges in the basin can collect point data for rain falling to the surface, but the model calculation needs rainfall data over the whole basin. Therefore, the observed rainfall point data is converted into basin areal rainfall by spatial interpolation.

In this study, the inverse distance weighted interpolation method (Chen, 2009, 2018) is used to calculate the spatial interpolation of rainfall in the river basin.

$$Z = \frac{\sum_{i=1}^{n} \frac{1}{(D_i)^P} z_i}{\sum_{i=1}^{n} \frac{1}{(D_i)^P}} \quad (4)$$

where Z is the property value of the estimated point; n is the number of points in the domain; $1/(D_i)^P$ is the weight value of the ith point on the estimated point; D_i is the distance, dm; and P is the power of distance, where the larger the value of P is, the faster the weight decays with distance. The power exponent P can be optimized based on the principle of minimum root mean square error.

Rainfall and soil moisture before flood events are the key factors affecting evapotranspiration in the basin. The vegetation evaporation is calculated as follows:

$$\begin{cases} E_i = VI_i^{t+\Delta t} - VI_i^t - P \\ S_{\max} = r \times L_{ai} \times F \end{cases} \quad (5)$$

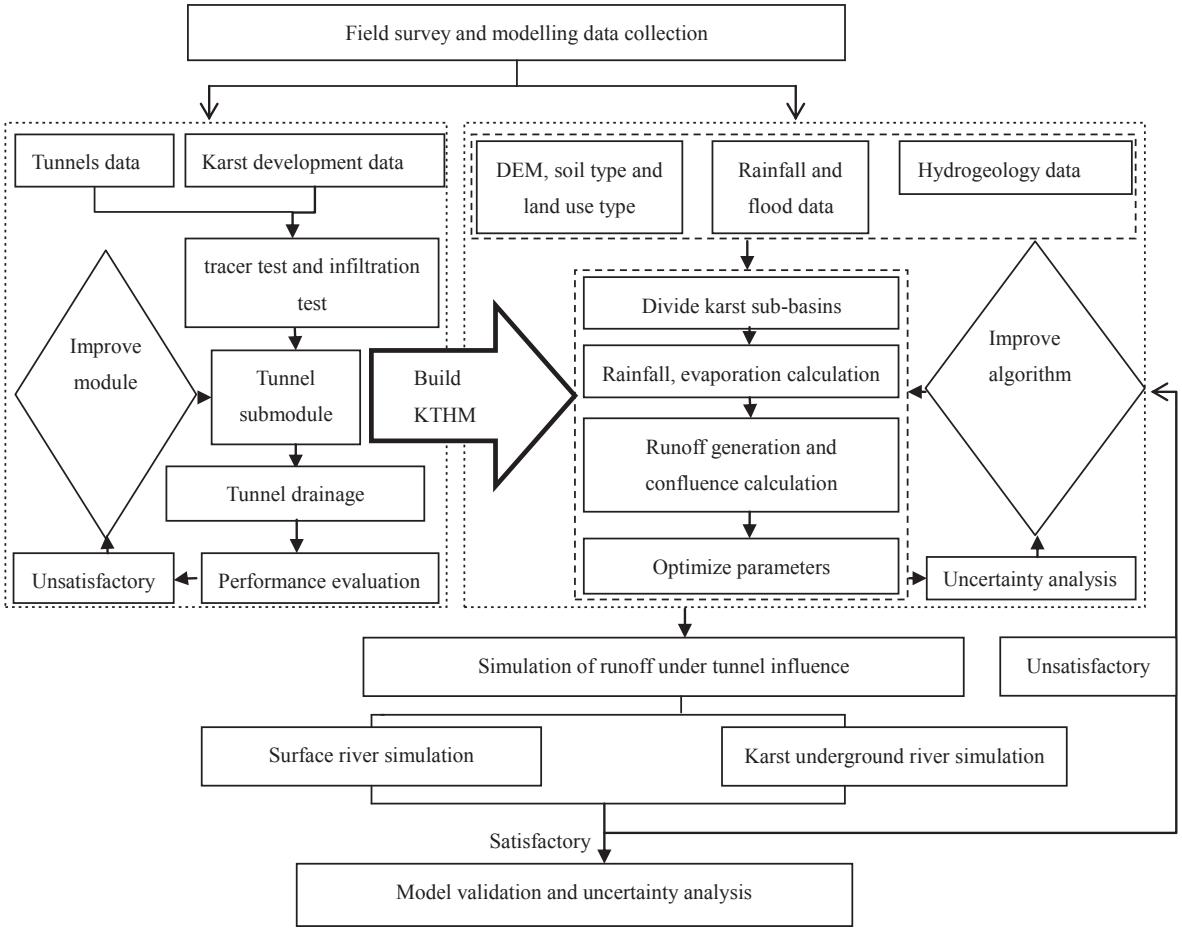

Fig. 2. Modelling and calculation flow chart of the KTHM.

where E_i is the vegetation evaporation, mm; $VI_i^{t+\Delta t} - VI_i^t$ is the variation in rainfall interception in the vegetation canopy, mm; P is the rain falling on the leaves, mm; S_{max} is the maximum interception of vegetation; r is the vegetation interception coefficient; L_{ai} is the leaf area index; and F is the canopy coverage.

Watershed soil evapotranspiration and phreatic water evaporation are calculated by the following equation (Chen, 2018):

$$\begin{cases} E_s = \lambda E_p, \ if \ S = S_c \\ E_s = \lambda E_p \frac{S}{F_c}, \ if \ S < S_c \\ E_g = \sum_{i=1}^{m} \frac{a^\gamma}{\Gamma(\gamma)} b^{\gamma-1} e^{-ab} \cdot \lambda E_p \left(1 - \frac{b}{D_m}\right) \frac{b}{i} \end{cases} \quad (6)$$

where

$$\begin{cases} a = \beta \frac{D_m}{D_o} \\ b = i \frac{D_{\max}}{m} \end{cases} \quad (7)$$

E_s is the current actual soil evapotranspiration, mm; λ is the evaporation coefficient, which can reflect the vegetational form, and $\lambda = 1 - C$, where C is the runoff coefficient and $\lambda = 1$ for the water surface; E_p is the potential evaporation, mm, which can be calculated by the water surface evaporation rate; S is the actual soil moisture content, mm; F_c is the field capacity; S_c is the saturated water content; E_g is the phreatic water evaporation, mm; m is the number of calculation cells; γ and β are the shape and scale parameters of the gamma function, respectively; D_o is the initial groundwater burial depth, dm; D_m is the average groundwater burial depth, dm; D_{max} is the maximum groundwater burial depth, dm; $\Gamma(\gamma)$ is the gamma function; a and b are the intermediate variables for calculation.

3.1.3. Rainfall runoff and confluence calculation

The horizontal structure of the KTHM includes river cells, hill slope cells, and reservoir cells. A hill slope cell in this study refers to an exposed karst slope landform cell, where runoff can be generated directly when the rainfall intensity is greater than the soil infiltration capacity. Runoff can be determined by subtracting subsoil seepage from net rainfall on the hill slope cells. Net rainfall refers to the amount of rain that percolates into the soil after plant interception and evapotranspiration, and the net rainfall on the slope cell can be described by the following equation:

$$\begin{cases} P_n(t) = \max\{0, [P_i(t) - E(t)]\} \\ E(t) = E_i(t) + E_s(t) + E_g(t) \end{cases} \quad (8)$$

where $P_n(t)$ and $P_i(t)$ are the net rainfall and rainfall at time t, respectively, mm; $E(t)$ is the evapotranspiration at time t, mm; and $E_i(t)$, $E_s(t)$, and $E_g(t)$ are the vegetation evaporation, soil evapotranspiration, and phreatic water evaporation, respectively, mm.

The net rainfall on the surface river cells refers to the amount of rain that falls directly into a river channel and plays an important role in the rainfall-runoff process. In particular, it affects the flow value in the outlet section of the basin and is combined with the river runoff in the confluence calculation. The net rainfall on each surface river cell can be calculated by the following equation (Bao et al.,2016):

$$P_r(t) = [P_i(t) - E_p] \frac{L_r \cdot R_{cw-\max}}{A} \quad (9)$$

where P_r and $P_i(t)$ are the net rainfall and rainfall at time t, respectively, on the rth surface river cell, mm; E_p is the potential evaporation, mm; L_r is the length of the rth river segment selected, dm; $R_{cw-\max}$ is the river width corresponding to the maximum river cross-section, dm; and A is

ARTICLE IN PRESS

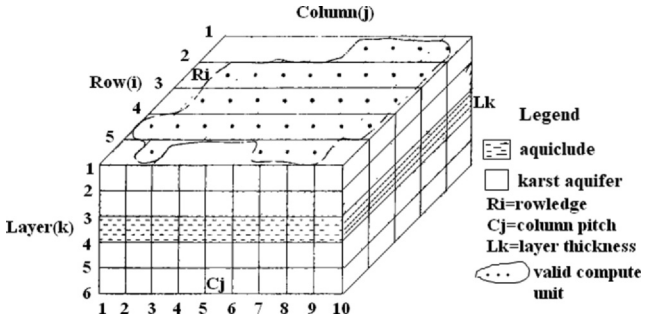

Fig. 3. Spatial arrangement of the karst aquifer.

the area of the surface river cell, dm^2.

The vertical structure of the KTHM has 5 layers: vegetation cover, soil layer, rock strata of the epikarst zone, bedrock, and the underground river system. When the net rainfall reaches the exposed karst slope cells, runoff can be generated if the rainfall intensity is greater than the soil infiltration capacity. This part of the runoff is called excess infiltration runoff in the KTHM. The rest of the net rainfall seeps into the soil in the surface karst zone, and the water quantity that infiltrates first compensates for any water shortage in the vadose zone. After the vadose zone is full, part of the water flows through the soil layer: the subsurface flow. The rest of the water continues to seep into the underground river system. In the KTHM, the depth of the surface excess infiltration runoff on slope cells and the underground runoff can be described by the following equation:

$$\begin{cases} R_{si} = (P_i - f_i),\ P_i \geqslant I_f \\ R_{si} = 0,\ P_i < I_f \\ I_f = \alpha(F_c - S)^{\delta} + S_f \\ R_{gi} = R_{0i}\exp(-at^b) \end{cases} \tag{10}$$

where R_{si} is the surface excess infiltration runoff depth on the slope cells at period t, mm; P_i and f_i are the net rainfall and amount of infiltration into the epikarst zone, respectively, mm; I_f is the infiltration capacity, mm, which varies in different karst landforms; α and δ are the parameters of the Holtan model; F_c is the field capacity, mm; S is the actual soil moisture content, mm; S_f is the steady infiltration water volume, mm; R_{gi} is the underground runoff depth at period t, mm; R_{0i} is the average depth of runoff that seeps into an underground water, mm; and a and b are constants based on the thickness of the karst aquifers and the soil infiltration capacity, which can be calculated by conducting a soil infiltration test based on the Holtan model in the study area.

The subsurface flow in the soil layer can be calculated by the following equation (Chen,2009):

$$\begin{cases} \frac{\partial Q_{lat}}{\partial x} + S_{fw}\cdot z\cdot\frac{\partial S}{\partial t} = Q_r - Q_{per} \\ Q_{lat} = v_{lat}\cdot S_{fw}\cdot z \\ v_{lat} = K\cdot\tan(\alpha),\ S > F_c \\ v_{lat} = 0,\ S \leqslant F \end{cases} \tag{11}$$

where Q_{lat} is the subsurface flow in the soil layer in the horizontal direction, L s^{-1}; v_{lat} is its flow velocity, m s^{-1}; Sfw is the width of the subsurface flow, m; z is the soil layer thickness, m; S and Fc are the soil water storage and field capacity, respectively; Qr is the runoff recharge at time t, L s^{-1}; Q_{per} is the seepage into the soil layer, L s^{-1}; K is the current soil hydraulic conductivity; and α is the hydraulic gradient of the subsurface flow.

In the epikarst zone, the distribution of small karst fissure systems is dominant, and the water movement pattern basically conforms to Darcy's law. Karst conduit systems have limited distribution, but the underground water flow can be laminar or turbulent. Thus, the karst water-bearing system in the epikarst zone can be generalized into a fissure system and conduit system. The former includes the rock matrix and very small cracks, while the latter includes the large karst voids and corrosion conduits. This generalization method is the same as that used in the CFPM1 module in the MODFLOW-CFP. In the KTHM, the infiltration water flow into the epikarst zone is considered carefully. In particular, the rules for the movement of infiltrated net rainfall and its transformation in the rock strata of the epikarst zone are refined. To describe runoff generation from net rainfall infiltration and confluence in water-bearing karst media, karst aquifers need to be discretized into small cuboid units according to the characteristics of the water-bearing karst media. The cuboid units can be further divided into L layers, and each layer includes M rows and N columns. The water head at the centre of the lattice represents that of the unit, and the permeation boundary is located at the unit edge. Considering that water movement in the epikarst zone basically conforms to Darcy's law, the confluence mode is basically consistent with the CFPM1 module in the MODFLOW-CFP. Therefore, in the model, this discrete method is revised from the MODLOW-CFPM1 module (Qin and Jiang, 2014). This discretized treatment of karst aquifers makes it easier for the model to effectively describe water movement within the units. Fig. 3 shows a cuboid unit of the simplified karst aquifer.

After the karst aquifer is discretized, to accurately simulate the water movement in the different water-bearing media in the karst aquifers, the karst water-bearing media need to be generalized effectively. In the KTHM, different generalization methods are adopted for the various karst media in the study area. For instance, the underground river system is generalized as a water-rich belt consisting of several connected large karst conduits, in which the flow is characterized as rapid flow (Li et al., 2019a, 2019b); fissured karst can be treated as an equivalent continuous medium; the water-rich zone in the epikarst zone can be generalized as a saturated medium with high permeability and large effective porosity; and caves are treated as anisotropic media with multiple holes and a large infiltration coefficient. These different generalization methods for karst media enable the KTHM to easily identify and simulate the water movement in karst aquifers.

In these cuboid units of the simplified karst aquifer, the valid computational unit (Fig. 3) is regarded as a dual medium that includes a porous medium and a very small fissure. When runoff flows into porous media, such as large karst caves and conduits, rapid underground runoff develops and quickly flows into the river channels of the subbasins. When the runoff passes through tiny karst fissures and small cracks, it forms slow underground runoff, which gradually collects into larger conduits and then drains into the underground river. In the cuboid unit of the simplified karst aquifer in the epikarst zone, the water flow from a unit to an adjacent low-gradient unit can be calculated by the following formula (modified form Zhang et al.,2009):

$$Q(t)_{ijk} = b_{ijk}\frac{\Delta h}{\Delta l}T(t)_{ij}R_iC_j \tag{12}$$

When water flows through tiny karst fissures, the hydraulic conductivity of slow underground runoff is as follows (Beven and Fisher, 1996):

$$T(t)_{ij} = nr\frac{\rho g R_i C_j L_k}{12v} \tag{13}$$

When water flows through a porous medium in karst aquifers, the hydraulic conductivity of the rapid underground runoff is as follows (Zhang et al.,2009):

$$T(t)_{ij} = \frac{K_{ij}(e^{-f_{ij}h_{ij}} - e^{-f_{ij}z_{ij}})}{f_{ij}} \tag{14}$$

where $Q(t)_{ijk}$ is the water flow from the cuboid unit to the adjacent low-gradient unit at time t, L s^{-1}; b_{ijk} is the runoff width of the cuboid unit ijk, m; $\frac{\Delta h}{\Delta l}$ is the hydraulic gradient, dimensionless; $T(t)_{ij}$ is the hydraulic conductivity, dimensionless; n is the number of karst fissures in the valid computational units; ρ is the density of flow, g L^{-1}; g is the gravitational acceleration, m s^{-2}; $R_iC_jL_k$ is the volume of cuboid unit

ijk, m^3; v is the kinematic viscosity coefficient; K_{ij} is the saturation permeability coefficient of the porous medium; f_{ij} is the attenuation coefficient of the vertical permeability of the soil; h_{ij} is the groundwater burial depth, m; and z_{ij} is the thickness of the epikarst zone, m.

Catchment confluence is the general term for the hydrological processes that lead various runoff pathways to converge into the outlet section of a river basin. In the KTHM, the calculation of runoff confluence includes the surface river confluence, hill slope confluence and underground river confluence. Among them, the surface river and hill slope confluence are calculated by the Saint-Venant equations, a one-dimensional wave movement equation is used for the hill slope confluence, and a diffusion wave movement equation is used for the confluence of the surface river. The confluence calculation processes involve the calculation of surface runoff confluence in the Liuxihe model (Chen, 2009, 2018). The confluence calculation process of karst underground rivers is described by using the Muskingum confluence model in the KTHM; this algorithm and its steps are described by Li et al. (2019a), Li et al. (2019b).

3.2. Model calibration and uncertainty analysis

The KTHM contains fifteen parameters (Table 2a). Among them, only the parameters with high and moderate sensitivities need to be optimized, and the insensitive parameters do not require optimization. The sensitivities of these parameters are calculated and evaluated in the following part of this paper. Ultimately, only ten parameters have to be optimized in the model, which improves the efficiency of the model calculation to a great extent. Table 2 lists the parameter set of the model.

The possible range of the initial values for some hydrogeological parameters in the study area must be determined before parametric optimization. For instance, the thickness and lithologic and stratigraphic properties of the epikarst zone can be obtained based on a field survey; the direction and distribution of karst underground river systems can be obtained by tracer tests in the study area; and the parameters related to rainfall infiltration can be obtained by infiltration experiments.

In the KTHM, an improved particle swarm optimization (PSO) algorithm (Chen et al., 2016) is employed to optimize the model parameters. After parametric optimization, the performance of the model in karst hydrological process simulations is verified; in this verification, the evaluation index of the simulation effect includes the correlation coefficient, relative flow process error, flood peak error and peak time difference and the water balance coefficient.

The uncertainty of the model simulation results is mainly based on three aspects. 1) Uncertainty of the model input data, such as rainfall and flow data and, more critically, hydrogeological data, which are more difficult to obtain in karst areas than in non-karst areas. 2) Uncertainty of the model structure itself, which is caused by systematic errors of the mathematical physical model. 3) Uncertainty of the model parameter optimization. In this paper, an improved PSO algorithm (Chen et al., 2016), which has been proven to effectively reduce the uncertainty of parameter transfer for distributed hydrological models, is used to optimize the parameters of the model (Li et al., 2017, 2019; Chen et al., 2017). In addition, the uncertainty of the model parameters can also be reduced by evaluating the sensitivity of the parameters.

In this study, a multiparametric sensitivity analysis algorithm (Choi et al., 1999; Li et al., 2019a, 2019b) is used to evaluate the sensitivity of the parameters in the KTHM, where the Nash–Sutcliffe coefficient is adopted as the objective function for the model calibration. Considering runoff simulation and forecasting, especially flood event forecasting, the simulation results of the flood peak flow are the most commonly used, so the minimum relative error of simulated peak flow is taken to calculate the Nash–Sutcliffe coefficient in this study:

Table 2
Parameters of the KTHM. List of model parameters.

Parameters	Name	Variable	Physical characteristics	Sensitivity
Rainfall Evaporation	Infiltration coefficient	I_c	Meteorology	Highly sensitive
	Potential evaporation	E_p	Meteorology	Insensitive
	Evaporation coefficient	λ	Vegetation cover	Moderately sensitive
	Wilting coefficient	W_c	Vegetation cover	Insensitive
Epikarst zone	Thickness	h	Soil type & karst attribute	Moderately sensitive
	Soil coefficient	S_b	Soil type	Highly sensitive
	Saturated water content	S_c	Soil type & karst attribute	Highly sensitive
	Rock porosity	R_p	karst attribute	Highly sensitive
	Field capacity	F_c	Soil type & karst attribute	Moderately sensitive
	Permeability coefficient	K	Soil type & karst attribute	Highly sensitive
Rainfall runoff Underground river	Flow direction	F_d	Landform	Highly sensitive
	Slope	S_0	Landform	Moderately sensitive
	Attenuation coefficient	A_c	Soil type & karst attribute	Insensitive
	Specific yield	S_y	Karst attribute	Highly sensitive
	Channel roughness	n	Landform & karst attribute	Moderately sensitive

b. Infiltration coefficients of rainfall on different karst landforms

Karst landform	Karst strongly developed	Karst moderately developed	Karst poorly developed
closed depression	0.62–0.78	0.40–0.65	0.25–0.38
not closed depression	0.41–0.60	0.32–0.40	0.18–0.25
monadnock, platform	0.22–0.40	0.23–0.31	0.21–0.24
hill slope	0.01–0.05	0.05–0.12	0.12–0.21

c. Hydrogeological parameters of the epikarst zone

Thickness/h	Saturated water content/S_c	Permeability coefficient/K	Rock porosity/R_p	Field capacity/F_c
(m)	(g cm^{-3})	(mm h^{-1})	(%)	(mm)
2.5–5.5	0.28–0.42	150–450	0.12–0.42	0.14–0.31

Table 3
Parameter sensitivity results for the KTHM.

Floods	Infiltration coefficient/I_c	Potential evaporation/E_p	Evaporation coefficient/λ	Wilting coefficient/W_c	Thickness/h
201905261200	0.93	0.36	0.54	0.12	0.67
	Soil coefficient/S_b	Saturated water content/S_c	Rock porosity/R_p	Field capacity/F_c	Permeability coefficient/K
	0.86	0.85	0.88	0.82	0.9
	Flow direction/F_d	Slope/S_0	Attenuation coefficient/A_c	Specific yield/S_y	Channel roughness/n
	0.77	0.65	0.44	0.8	0.62

$$E = 1 - \frac{\sum_{i=1}^{n} (Q_i - Q_i')^2}{\sum_{i=1}^{n} (Q_i - \bar{Q})^2} \quad (15)$$

where E is the value of the Nash–Sutcliffe coefficient; Q_i and Q_i' are the observed and simulated peak flows, respectively, L s^{-1}; $\bar{Q}$ is the average observed peak flow, L s^{-1}; and n is the number of observations.

The procedure for parameter sensitivity analysis of the KTHM involves the following steps:

(1) The initial parameter value range is set to [0.2, 3.0] according to the parameter properties. The convergence condition for parameter optimization is set to 10^{-4}, and the Nash–Sutcliffe coefficient threshold value is set to 0.9.
(2) Three thousand groups of initial parameter sets for each model parameter are acquired based on the Monte Carlo sampling method in the model (Li et al., 2019a, 2019b).
(3) The flow process is simulated by using these three thousand groups of parameters in the KTHM, and the Nash coefficients for each simulation are recorded.
(4) These Nash coefficient values are compared with the threshold of 0.9: if a coefficient is greater than 0.9, then it is considered an acceptable value; otherwise, it is considered an unacceptable value.
(5) Evaluating the degree of dispersion of the acceptable and unacceptable values implies the sensitivity of each model parameter.

3.3. Model setup

The model setting mainly refers to some initial value ranges and conditional assumptions before the simulation calculation, including the following points. (1) The initial soil moisture is set to 20–90% of the saturated soil water content during floods. However, the most suitable soil moisture content within this range in the early stage of flood needs to be determined by many model runs. (2) The groundwater divide and initial water head are determined by tracer experiments and flow field analysis of the karst aquifers in the study area. In the tunnel submodule, this groundwater divide is the boundary of the complete hydrogeological unit, across which the tunnel passes. In the dry season, the flow in karst conduits in the tunnel site area is small, so the tunnels in this study area can be used as temporary dynamic head boundaries. (3) The flow direction and distribution of underground rivers in the study area are also deduced by tracer experiments, where the water level and flow are monitored in real time by an automatic water station at the outlet of the underground river. The river base flow is 60 L s^{-1} according to the perennial average dry season runoff. (4) The initial value range of the model parameters must be set to optimize the parameters. (5) The DEM, land use, soil and flow data are input to the KTHM to verify its performance in karst hydrological simulations. The hydrological effects of tunnel drainage can be determined through the simulated water volume difference between the KHM (without the tunnel submodule) and the KTHM.

According to the characteristics of karst development in the underlying rocks of the basin, 1267 karst subbasin units, including 372 river cells, 836 hill slope cells, and 59 reservoir cells, are identified based on the 15 m × 15 m DEM. The bottom plate of the tunnel submodule is set to an elevation of 0 m in the simulations, and its dimensions are a length of 4035 m and a thickness of 8 m. The karst aquifer in the tunnel site area is generalized as cuboid units (Fig. 3), where they are divided into 179 layers, 465 rows and 625 columns.

4. Results

4.1. Results of the parametric sensitivity analysis

The parameter sensitivity analysis is performed to evaluate the sensitivity of each parameter and determine the highly sensitive, moderately sensitive and insensitive parameters in the KTHM. In parametric optimization, only highly and moderately sensitive parameters must be optimized, and insensitive parameters do not require optimization; thus, the efficiency of the model calculation can be considerably improved. The sensitivity analysis of the model parameters is calculated by Eq. (15), where flood peak flow is used as the state variable in the parameter sensitivity analysis, and the results are listed in Table 3.

The results of the parameter sensitivity in Table 3 show that the calculated values are all between 0 and 1. The closer the value is to 1, the greater the sensitivity of the parameter. We set calculated value intervals to categorize the sensitivity of parameters: a calculated value between 0.7 and 1 is considered a highly sensitive parameter; the calculated value of a moderately sensitive parameter is between 0.45 and 0.7; and a calculated value less than 0.45 is considered insensitive. Therefore, the highly sensitive parameters in the KTHM are the infiltration coefficient I_c, permeability coefficient K, rock porosity R_p, saturated water content S_c, field capacity F_c, specific yield S_y and flow direction F_d; the insensitive parameters are the attenuation coefficient A_c, potential evaporation E_p, and wilting coefficient W_c. The remaining model parameters are moderately sensitive.

The order of parameter sensitivity is as follows: infiltration coefficient I_c > permeability coefficient K > rock porosity R_p > saturated water content S_c > field capacity F_c > specific yield S_y > flow direction F_d > thickness h > slope S_0 > channel roughness n > evaporation coefficient λ > attenuation coefficient A_c > potential evaporation E_p > wilting coefficient W_c.

4.2. Results of model parametric optimization

Twenty flow processes and two annual runoffs are chosen to verify the results of the KTHM hydrological simulations in karst. Among them, four flows, including flows 201804210800, 201809100345, 201905261200 and 201907261200, are selected for model parametric optimization, and floods with the optimal simulation effect are used for the final parameter optimization. These four typical flow processes can basically represent all flow conditions in the research area, where flow 201804210800 represents dry season runoff; flows 201809100345 and 201905261200 represent normal runoff; and flow 201907261200 represents flood runoff. The remaining flows are used to validate the performance of the KTHM. The KTHM has a total of 15 parameters, among which only the 10 parameters with high and moderate sensitivities need to be optimized. The parametric optimization results of the KTHM are shown in Fig. 4.

The parametric optimization results in Fig. 4 illustrate that the model parameters and their objective functions converge after 20 iterations and that the sensitivities of the parameters remain constant

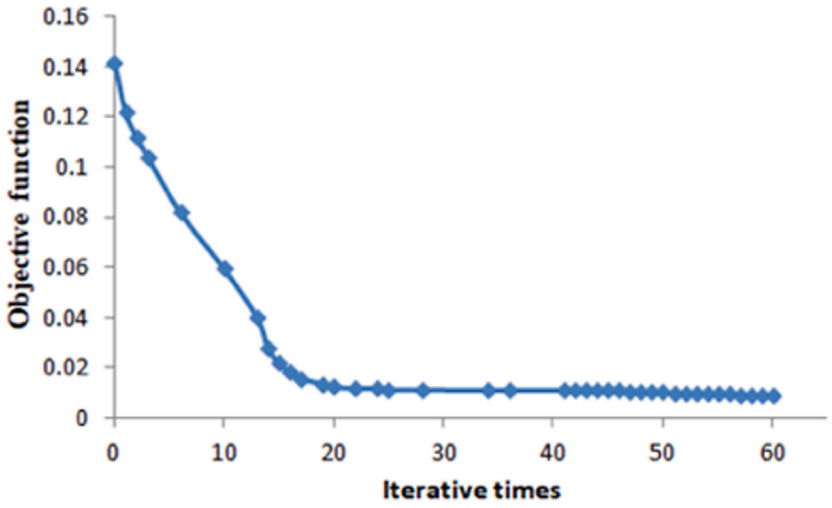

a. Evolution process of the objective function in parameter optimization

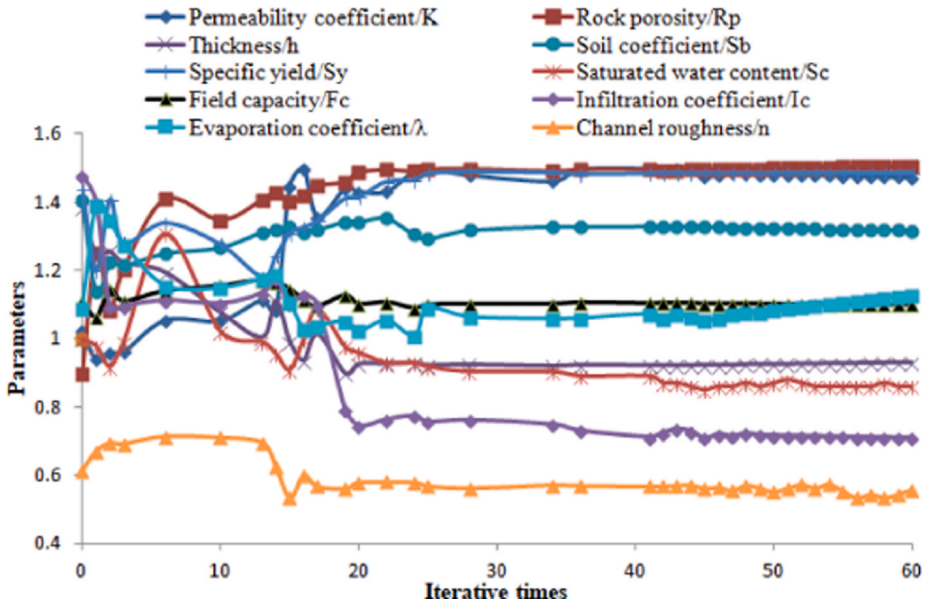

b. Evolution results for the model parameters

Fig. 4. Parametric optimization results of the KTHM.

after 60 iterations, which implies that the computational efficiency of the model is very high. To verify the simulation effects of the model on different hydrological processes, dry season runoff, normal runoff and flood events are used to calibrate the model parameters in this study. Fig. 5 shows the flow simulation effects based on the parameter optimization.

In Fig. 5, the simulated effects based on the KTHM are satisfactory for all the hydrological processes, and the KTHM performs better than the KHM in runoff simulations, especially the simulated peak flows, which demonstrates that the tunnel submodule in the KTHM is effective. The good simulation results indicate that the improved PSO algorithm chosen in the parametric optimization of the KTHM is feasible.

The results from the simulations of the four flows in Fig. 5 show that the best simulated effect is obtained for normal flow 201905261200: the overall simulation effect of this multipeak flood is the best. Therefore, the parameter results corresponding to flow 201905261200 are used as the optimal parameter set to simulate and verify the remaining nineteen flow processes and 2 annual runoffs.

To further verify the results of parameter optimization, five evaluation indices for the simulated flow effects, including the correlation coefficient, the relative flow process error, the flood peak error and its peak time difference and the water balance coefficient, are calculated and listed in Table 4.

The simulated flow effects in Table 4 reveal that compared with the performance of the KHM, the KTHM presents more accurate results and superior evaluation indices from flow simulations. With the KTHM, the correlation coefficient increases by 14%, the relative flow process error decreases by 9%, the flood peak error decreases by 12%, the water balance coefficient decreases by 27%, and the peak time error decreases by 2 h compared to the results of the KHM. The best simulated evaluation indices are obtained for normal flow 201905261200, which is the same result as shown in Fig. 5.

4.3. Model validation in runoff simulations during the year

Nineteen flow processes during the year, including floods, normal runoff, and dry season runoff at the outlet of the underground river, are used to verify the performance of the KTHM. To describe the effects of

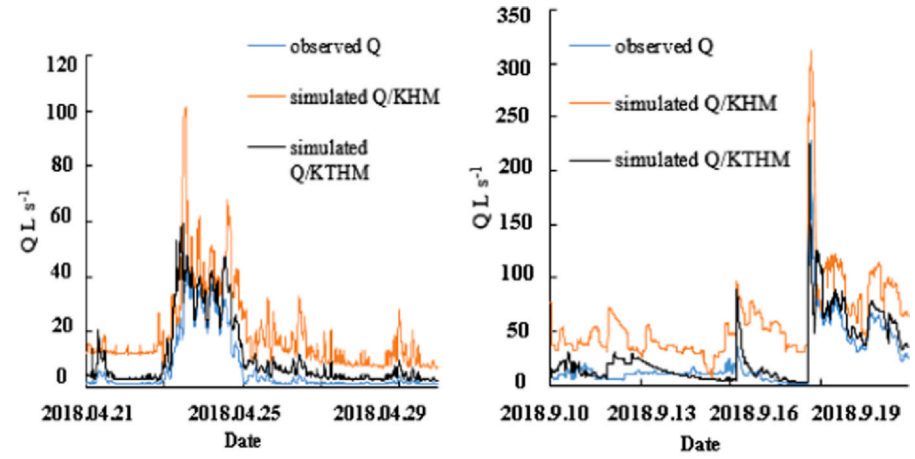

a. flow 201804210800 b. flow 201809100345

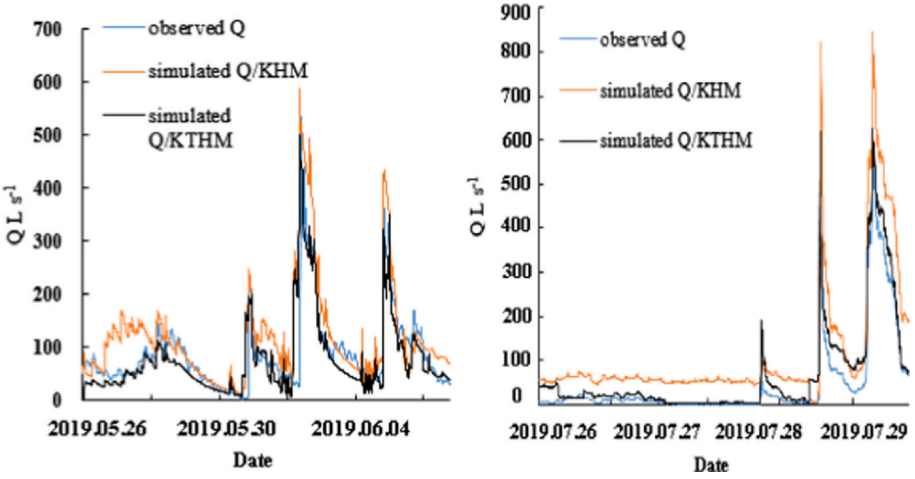

c. flow 201905261200 d. flow 201907261200

Fig. 5. Flow simulation effects based on the parameter optimization.

Table 4
Evaluation indices of the flood simulations by parametric optimization.

Flows	Models	Correlation coefficient/R	Relative flow process error/P%	Flood peak error/E%	Water balance coefficient/W	Peak time error/T (hours)
201805081200	KHM	0.75	17	19	1.17	3
	KTHM	0.90	11	10	0.92	2
201809100345	KHM	0.76	18	22	1.29	4
	KTHM	0.89	13	10	0.93	2
201812221800	KHM	0.79	19	25	1.23	5
	KTHM	0.92	10	8	0.92	2
201905261200	KHM	0.77	19	14	1.09	−5
	KTHM	0.94	8	6	0.94	−3
Average values	KHM	0.77	19	20	1.20	3
	KTHM	0.91	10	8	0.93	1

the tunnel submodule in the model, the flow simulation results determined by the KHM and KTHM, are compared in Fig. 6; however, only six of the flow process simulation results are shown here due to space limitations. Among them, each has two flows representing flood runoff, normal runoff and dry season runoff.

The simulated flow results in Fig. 6 illustrate that the simulated flow processes based on the KTHM are much more accurate than those based on the KHM. The flow simulation values of the KHM are larger than the observed values, while the flow values simulated by the KTHM are very close to the observed values. These results are consistent with those of the four flows used in parametric optimization and confirm that adding the tunnel submodule to the KHM to develop the KTHM is necessary.

To further compare the simulated flow results based on the KHM and KTHM, five evaluation indices of all nineteen flows are used to assess the simulated effects, as listed in Table 5.

In Table 5, the average values of the correlation coefficient, relative flow process error, flood peak error, water balance coefficient, and peak flow time error based on the KHM are 0.73, 29%, 30%, 1.16 and −6 h, respectively, whereas the average values of these five evaluation indices based on the KTHM are 0.95, 11%, 6%, 0.94 and −3 h, respectively. These findings indicate that all the evaluation indices from the KTHM are more accurate than those from the KHM. Thus, the tunnel

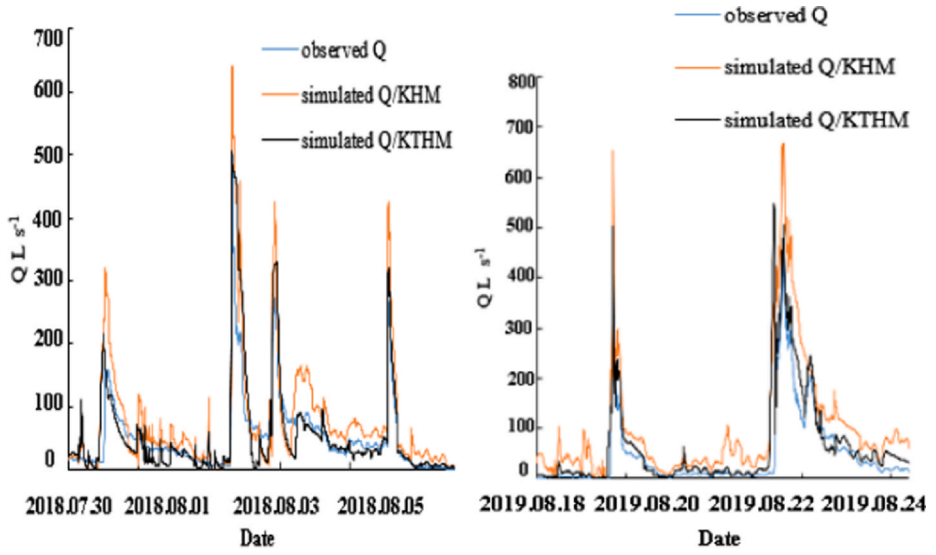

a. flood 201807301100 b. flood 201908181400

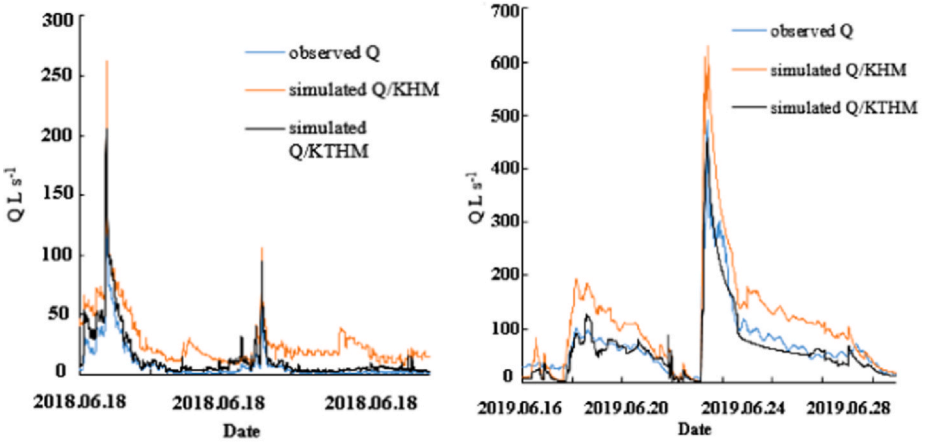

c. normal runoff 201806181200 d. normal runoff 201906161400

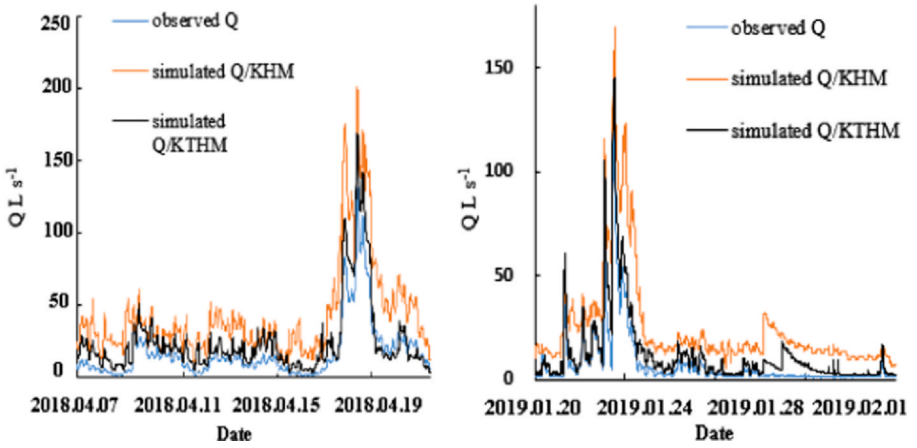

e. dry season runoff 201804071200 f. dry season runoff 201901200130

Fig. 6. Flow process simulation effects based on the KHM and KTHM.

submodule designed in the model is effective, and the KTHM proposed in this study is feasible for flow simulations in karst areas.

The difference between the water amounts simulated by the KHM and KTHM represents the water loss caused by tunnel engineering in the study area. The simulated water volume can be determined by the area enclosed by the flow process lines and the time axes. Table 6 shows the calculated results of the water volume difference between the KHM and the KTHM in a year.

In Table 6, the differential ratio (%) refers to the ratio of the difference between the simulated peak flow or total flood volume of the

ARTICLE IN PRESS

Table 5
Evaluation indices of the flood simulations for model validation.

Floods	Model types	Correlation coefficient/R	Relative flow process error/P%	Flood peak error/E%	Water balance coefficient/W	Peak time error/T (hours)
201804071200	KHM	0.78	31	32	1.21	−5
	KTHM	0.96	12	6	0.96	−1
201804210800	KHM	0.79	21	21	1.18	−3
	KTHM	0.98	12	−10	0.93	−2
201804271400	KHM	0.67	28	36	1.04	−6
	KTHM	0.92	13	11	0.95	−3
201805081200	KHM	0.69	28	41	1.16	−4
	KTHM	0.93	9	8	0.93	−2
201805240800	KHM	0.69	23	14	1.33	−6
	KTHM	0.91	14	−4	0.89	−4
201806071200	KHM	0.76	33	29	1.11	−2
	KTHM	0.95	12	−4	0.95	−1
201806181200	KHM	0.75	28	23	1.08	6
	KTHM	0.92	11	4	0.89	2
201807301100	KHM	0.61	30	24	1.1	−7
	KTHM	0.91	12	−3	0.95	−4
201809100345	KHM	0.75	29	49	1.23	6
	KTHM	0.98	9	6	0.87	2
201809301100	KHM	0.72	29	27	1.36	−6
	KTHM	0.93	13	−7	0.93	−4
201810151030	KHM	0.75	31	25	1.09	−6
	KTHM	0.97	13	−7	0.91	−2
201812221800	KHM	0.72	26	21	1.13	6
	KTHM	0.98	10	−4	0.97	3
201901200130	KHM	0.79	31	17	1.25	5
	KTHM	0.93	12	5	0.93	2
201905121400	KHM	0.68	28	16	1.03	−7
	KTHM	0.95	14	−3	0.93	−3
201905261200	KHM	0.72	29	40	1.11	7
	KTHM	0.93	10	7	0.96	3
201907061500	KHM	0.73	35	40	1.09	4
	KTHM	0.98	10	7	0.95	2
201907261200	KHM	0.75	32	47	1.14	−6
	KTHM	0.95	8	5	0.95	−3
201908181400	KHM	0.67	31	40	1.2	−4
	KTHM	0.96	11	3	0.95	−2
201906161400	KHM	0.78	31	34	1.17	−8
	KTHM	0.95	12	−5	0.97	−4
201910171600	KHM	0.91	28	13	1.15	−6
	KTHM	0.95	11	−4	0.96	−3
average value	KHM	0.73	29	30	1.16	−6
	KTHM	0.95	11	6	0.94	−3

Table 6
The average values of simulated water volume difference based on the KHM and the KTHM.

Types	Model types	Peak flow (L s^{-1})	Differential ratio (%)	Water volume (L)	Differential ratio (%)
Flood runoff	Observed value	543		189,260	
	Simulated/KHM	617		203,680	
	Simulated/KTHM	532	16	181,033	12
Normal runoff	Observed value	357		118,286	
	Simulated/KHM	430		143,951	
	Simulated/KTHM	342	25	118,950	21
Dry season runoff	Observed value	128		41,280	
	Simulated/KHM	171		52,164	
	Simulated/KTHM	134	29	42,225	24

models to the observed value. This value is the proportion of water loss caused by the tunnels of the observed water volume, which reflects the influence of the tunnels on the water volume of the runoff at the underground river outlet. The results in Table 6 show that the peak flows and water amounts simulated by the KHM are larger than the observed values, while the simulated values of the KTHM are close to the observed values. The average differential ratios for the flood peak flow and the flood water volume are 16% and 12%. The simulated peak flow and water volume of the normal runoff are 25% and 21% of the observed values, whereas simulated peak flow and water volume of the dry season runoff are 29% and 24%. These findings indicate that the influence of a tunnel is greater on the peak flow than on the water volume and that a tunnel has the greatest influence on the dry season runoff and the least influence on the flood runoff among the runoff categories. Moreover, the sensitivity of the hydrological effects of tunnels follows the order of water volume of dry season runoff > normal runoff volume > flood peak flow > flood volume.

4.4. Interannual runoff simulation results

Runoff during the year is divided into flood, dry season runoff and normal runoff according to the amount of water. The KTHM works well

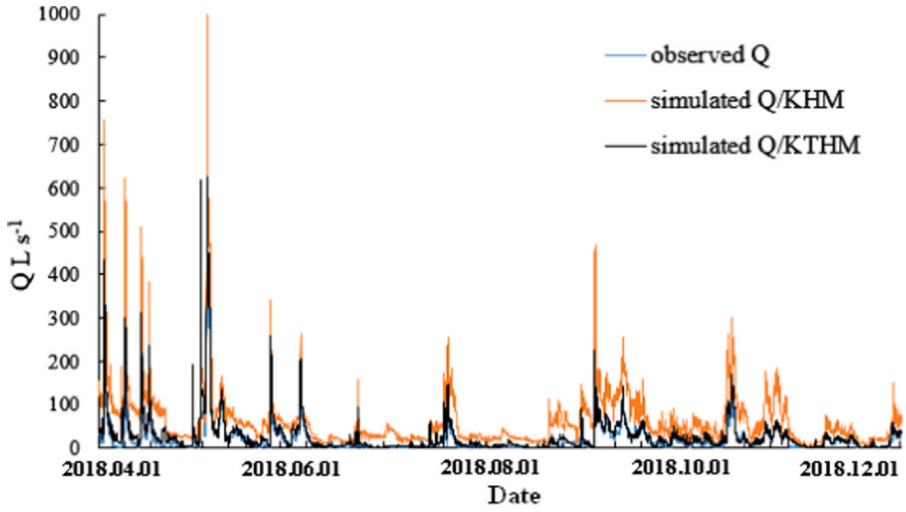

a. Annual runoff simulated effect of 2018

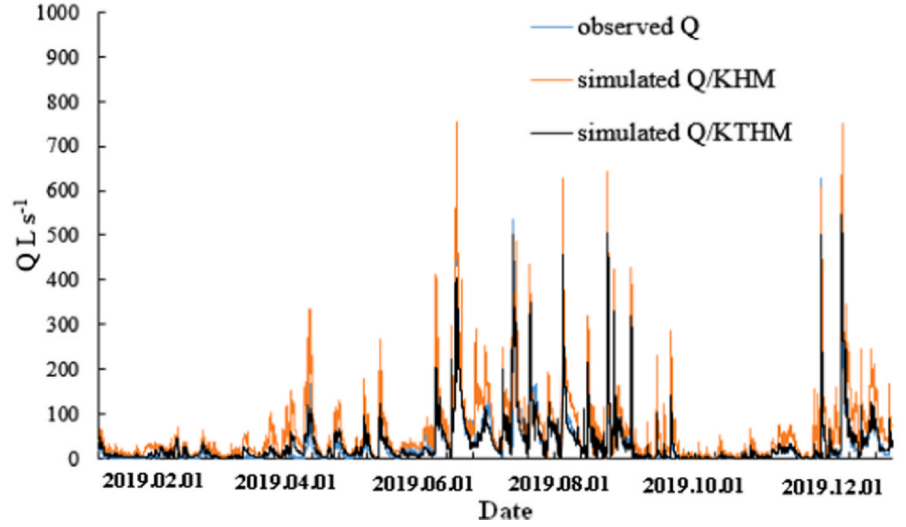

b. Annual runoff simulated effect of 2019

Fig. 7. Annual runoff simulated effects based on the KHM and KTHM.

Table 7
Evaluation indices of interannual runoff simulated by the KHM and KTHM.

Floods	Model types	Correlation coefficient/R	Relative flow process error/P %	Flood peak error/E%	Water balance coefficient/W	Peak time error/T (hours)
2018 annual runoff	KHM	0.75	22	35	1.25	5
	KTHM	0.92	11	9	0.94	3
2019 annual runoff	KHM	0.78	25	28	1.18	−4
	KTHM	0.95	19	6	0.92	−2
average value	KHM	0.77	24	32	1.22	5
	KTHM	0.94	15	8	0.93	2

for runoff simulations throughout a year. To further validate the performance of the new KTHM for interannual runoff simulations, 2 annual runoffs (2018 and 2019) are simulated by the KTHM in this study. Fig. 7 shows the flow simulated effects by the KHM and KTHM, and Table 7 lists their evaluation indices.

The results of the 2 annual runoff simulations from the KHM and KTHM shown in Fig. 7 and Table 7 indicate that the KTHM results are more accurate for interannual runoff simulations than the KHM results. In particular, the simulation effects of almost every peak flow in the annual flow processes by the KTHM are very close to the observed values, and the average value of the simulated peak flow error is only 8%. In contrast, the simulation effect of the KHM for each peak flow is poor; the simulated value is much larger than the observed value, with an average simulated peak flow error of 32%. Thus, the tunnel submodule designed in the KTHM is effective and necessary. This finding is consistent with the results previously discussed in Section 4.3.

To describe the impact of tunnel engineering on the water volume of interannual runoff, the water volume of 2 annual runoffs is simulated by the KHM and KTHM and listed in Table 8.

Table 8 shows that the water volumes of the interannual runoff simulated by the KHM are larger than those of the observed values and that the average relative error between the simulated value and the

ARTICLE IN PRESS

Table 8
Water volume of interannual runoff simulated based on the KHM and KTHM.

Annual runoff	Model types	Water volume (L)	Relative error (%)	Water volume difference (L)	Differential ratio (%)
2018	Observed value	1,139,217			
	Simulated/KHM	1,295,040	14		
	Simulated/KTHM	1,087,500	−5	207,540	18
2019	Observed value	1,199,080			
	Simulated/KHM	1,355,080	13		
	Simulated/KTHM	1,109,800	−7	245,280	20
Average value	Observed value	1,169,149			
	Simulated/KHM	1,325,060	13		
	Simulated/KTHM	1,098,650	−6	226,410	19

observed value is 13%; however, the interannual runoff volume simulated by the KTHM is more accurate, and the average relative error is only −6%. Moreover, the average differential ratio is 19% with the KTHM. A comparison of the results of the effect of a tunnel on the flow processes within a year (Table 6) shows that the influence the tunnel on the flow processes within a year is greater than that of the interannual runoff.

5. Discussion

5.1. Effects of tunnel excavation on groundwater flow processes

The simulated runoff results during the year (Fig. 6) and the annual runoff (Fig. 7) show that the flow processes at the outlet of the underground river simulated by the KHM and the KTHM are reliable. Moreover, the flow process lines of the simulations by the KHM and KTHM are generally consistent with the observed values. However, the average relative flow process error (P%) of simulated runoff during the year is 29% with the KHM and 11% with the KTHM (Table 5), and the interannual runoff is 24% with the KHM and 15% with the KTHM (Table 7). In addition, the hydrological effects of tunnel engineering on the flow processes are considerable, as indicated by the relative error between the flow processes simulated by the KHM and the observed processes. This result is reliable because the KHM and the KTHM are actually the same model, and the only difference is that a tunnel submodule is not included in the KHM. Since the simulation results of the same model are compared, the systematic errors inside the model can be ignored.

The influence of tunnel engineering in karst areas on flow processes is also reflected in flood detention. During a flood, tunnel drainage removes some of the water that should be discharged from the underground river outlet, thus leading to a time lag of the flood peak. In Table 5, the peak time errors (T) with the KHM and KTHM are −6 and −3 h, respectively. These findings show that the tunnels in the study area caused the flood peak of the underground river to appear 3 h later. The flood detention effect of tunnels should be considered in future flood forecasting in the research area.

5.2. Effects of tunnel excavation on groundwater quantity

The hydrological effects of tunnelling on runoff mainly occur through the influence of tunnel engineering on runoff quantity. The results of 19 flow processes and 2 annual runoffs simulated with the KHM and the KTHM show that the simulated values of floods, normal runoff and dry season runoff as well as 2 annual runoffs are larger than the observed values when utilizing the KHM, while those simulated values by the KTHM are basically consistent with the observations (Tables 6 and 8). This difference is because the KHM does not consider tunnel drainage in the study area; therefore, according to the principle of water balance, some of the water that should drain from the tunnels is added to the flow at the outlet of the underground river. As a result, the flows simulated by the KHM are larger than the observed values. When the tunnel submodule is added in the KTHM to simulate the flow processes, the simulated values are completely consistent with the observed values. This finding indicates that the calculation of the actual water volume of the basin in the KTHM is basically balanced. However, the KTHM underestimates the flood runoff, normal runoff (Table 6), and interannual runoff (Table 8) but overestimates the dry season runoff (Table 6). The errors of water quantity overestimation or underestimation are not large and thus may be caused by the systematic error of the model.

The simulation results for runoff during a year (Table 6) and interannual runoff (Table 8) show that the influence of the tunnels on the peak flow is greater than that on its water volume. In addition, the influence of tunnel engineering in karst areas on the runoff quantity during a year is greater than that of interannual runoff. This is because the simulation results of the interannual runoff balance the water volume difference between the flood and dry season runoff. The results in Table 6 show that tunnels in karst areas have the greatest influence on the water volume of runoff in the dry season (24%) and the least influence on flood runoff (12%). This is because the shape and size of the tunnels are fixed, the corresponding drainage is usually fixed within a certain range, and the water loss by tunnels accounts for a large proportion in the dry season runoff, decreasing the dry season runoff. In contrast, tunnel water loss accounts for a small proportion of the flood water volume and has little impact on it. The sensitivity sequence of hydrological effects of tunnels is as follows: water volume of dry season runoff > normal runoff volume > water volume of interannual runoff > flood peak flow > flood volume.

In summary, tunnel engineering in the study area has a great influence on natural karst runoff. Tunnels can reduce the discharge flow at the underground river outlet and delay the occurrence time of peak discharge. Tunnels have a great influence on runoff during the dry season, and the underground rivers in this area were initially perennial. However, these rivers were cut off seasonally after tunnel construction. Tunnel excavation also leads to serious surface water leakage and groundwater drainage problems; in the study area, a large area of paddy fields is now abandoned dry land. Local residents have to drill wells more than 117 m deep to obtain a reasonable water supply. A certain range of karst rocky desertification forms due to surface water leakage. Tunnel engineering in karst areas has caused almost irreversible damage to the originally fragile karst water system and ecological environment.

5.3. Uncertainty analysis of simulation results

The uncertainty of the model simulation results is due to mainly the following three aspects. First, there may be uncertainties in the acquisition mode and data reliability of the model input data. In particular, it is difficult to obtain reliable hydrogeological data in karst areas. Regarding the meteorological, hydrological and geological data used to build the KTHM in this study, three types of reviews must be conducted

before the values are input into the model: a reliability review of data sources and consistency and representative evaluations of the data. For the pretreatment process for these data, our previous research results can be referenced (Li et al., 2019a, 2019b). Second, as a mathematical-physical model, the distributed hydrological model structure may be uncertain due to systematic errors, which are mainly reduced by simplifying the model structure and improving the algorithm. For instance, the underground confluence module is divided into only two layers, the confluence of the epikarst zone and the underground river system, and the algorithms of slow and rapid flow in karst water-bearing media are improved effectively (Eqs. (12)–(14)). Third, uncertainty arises during model parameter optimization. There are many parameters in a distributed hydrological model, which leads to some uncertainty in parameter optimization.

In this study, we reduce the uncertainty of model parameters in two ways. First, an improved PSO algorithm is used to automatically optimize the model parameters, which can reduce the uncertainty of parameter transfer in the model effectively. Second, parametric sensitivity analysis is performed to reduce uncertainty. We calculate the sensitivity of each parameter of the KTHM in detail (Table 3), and the sensitivity of the model parameters is divided into highly sensitive, moderately sensitive and insensitive. When parameters are optimized, only the highly and moderately sensitive parameters need to be calculated, while the insensitive parameters do not need to be optimized, which improves the computational efficiency of the model.

From the results of the parametric sensitivity analysis in Section 4.1, the parameters related to the infiltration characteristics and karst water-bearing medium are highly sensitive, while the model parameters associated with evapotranspiration and wilting coefficient are not sensitive. This shows that the karst hydrogeological characteristics, especially those of an anisotropic karst aquifer, have the greatest influence on the parameters of the distributed hydrological model, which controls the movement and transformation of infiltration water in karst water-bearing media. However, parameters such as evapotranspiration in the basin are insensitive, indicating that the water loss by evaporation has little influence on the quantity of water at the underground river outlet in the study area, especially during the flood season, and that the proportion of evapotranspiration from the flood water is very small.

By evaluating the uncertainty of the model simulation results, the errors of the hydrological simulation in the model karst can be greatly reduced, and the accuracy can be well improved. The KTHM developed in this study is applicable in the study area, and the mechanism of this KTHM is suitable for performing hydrological simulation of a variety of karst landforms because the runoff generation and confluence module in the model includes the excess infiltration runoff and runoff generation under saturated conditions (Eqs. (10) and (11)). When the model is applied to exposed karst areas, the rainfall runoff can be calculated by using the excess infiltration runoff module, while in buried karst basins, it can be described by runoff generation under saturated conditions. The results of this study provide a good tool for the hydrological simulation and hydrological effect analysis of tunnels in karst areas.

6. Conclusions

Tunnel engineering in the study area has a great impact on the natural karst hydrological process according to the field survey. Therefore, building a hydrological model to stimulate the hydrological effects of tunnels is necessary. However, the complicated underlying surface conditions and heterogeneous aquifer interactions in the study area pose great challenges for the application of hydrological models and make it difficult to accurately describe the water movement and transformation in karst water-bearing media. In addition, the current distributed hydrological models usually need a considerable amount of hydrogeological data when used in karst areas due to the variety of structures and range of parameters. To overcome the challenge of applying a distributed model in the study area, a new fully distributed KTHM is proposed in this study to investigate the hydrological effects of tunnels. The following conclusions are based on the research results:

(1) The parameters related to the infiltration and karst water-bearing medium in the KTHM are highly sensitive, while those related to the evapotranspiration are insensitive. The order of parameter sensitivity is as follows: infiltration coefficient I_c > permeability coefficient K > rock porosity R_p > saturated water content S_c > field capacity F_c > specific yield S_y > flow direction F_d > thickness h > slope S_0 > channel roughness n > evaporation coefficient λ > attenuation coefficient A_c > potential evaporation E_p > wilting coefficient W_c.
(2) The improved PSO algorithm is effective for parametric optimization of the KTHM and can considerably increase the computational efficiency of the model, and the model parameters and their objective functions converge after only 20 iterations. Comparing the performances of the KHM and KTHM in flood simulations with parametric optimization, the KTHM is more accurate than the KHM; the correlation coefficient increases by 14%, the relative flow process error decreases by 9%, the flood peak error decreases by 12%, the water balance coefficient decreases by 27%, and the peak time error decreases by 2 h.
(3) The simulated flood results from the KTHM are more accurate than those from the KHM, especially the simulated peak flows. The 5 evaluation indices improve considerably when the KTHM is used; the average values of the correlation coefficient, relative flow process error, flood peak error, water balance coefficient, and peak flow time error based on the KHM are 0.73, 29%, 30%, 1.16 and −6 h, respectively, whereas the average values of these five evaluation indices based on the KTHM are 0.95, 11%, 6%, 0.94 and −3 h, respectively. Clearly, the evaluation indices of the KTHM indicate that this approach is considerably more accurate the KHM, suggesting that the tunnel submodule is effective and that the KTHM proposed in this study is feasible for performing flood simulations in the study area.
(4) The water volume difference between the KHM and the KTHM represents the water loss caused by the tunnels in the study area. The simulated water difference indicates that tunnel engineering in the study area has a great influence on the runoff at the outlet of underground rivers. The influence on the runoff during a year is greater than that of interannual runoff, and its influence on the peak flow is greater than that on its water volume. In the study area, tunnels have the greatest impact on runoff during the dry season by reducing the runoff volume, which leads to seasonal interruptions in underground river flow. Tunnels have little influence on flood runoff. The sensitivity sequence of the hydrological effects of tunnelling is as follows: water volume of dry season runoff > normal runoff volume > water volume of interannual runoff > flood peak flow > flood volume.
(5) These reasonable flow simulation results in the study area show that the KTHM model developed in this paper is feasible for karst hydrology simulation and that the tunnel submodule in the model can effectively describe the drainage of tunnels. Because of the simple structure of this KTHM, it is easy to build models to represent other karst basins with tunnels similar to the Zhongliangshan karst basin. Therefore, this model has great application potential in karst areas. Considering that several additional tunnel projects will be constructed in the research area, this KTHM can be built in advance to predict the possible drainage conditions of the tunnel, which will be very helpful for the tunnel engineering design and can provide strong theoretical and data support.

7. Data availability

All data used in this paper are available, findable, accessible,

interoperable, and reusable (FAIR).

The DEM is downloaded from the Shuttle Radar Topography Mission database at http://srtm.csi.cgiar.org (last access: 12 Jan 2020). The initial spatial resolution of the DEM is 30 m × 30 m; the land use data are downloaded from http://landcover.usgs.gov (last access: 10 Jan 2020), and the soil data are downloaded from http://www.isric.org (last access: 10 Jan 2020).

Author contributions

JIL is the first author and is responsible for the calculations and writing the whole paper. AH provided the data on rainfall and flooding. DY provided advice on the scientific issues raised in this article. YJ is the corresponding author who helped conceive the structure of the model. SD and CC helped revise the paper. JL provided significant assistance in the English translation of the paper.

Declaration of Competing Interest

The authors declare that they have no known competing financial interests or personal relationships that could have appeared to influence the work reported in this paper.

Acknowledgements

This study is supported by the National Key Research and Development Program of China (2016YFC0502306), the Chongqing Municipal Science and Technology Commission Fellowship Fund (ctsc2017jcyj-ysxX0004, cstc2018jcyj-yszx0013, and cstc2019yszx-jcyjX0002), the China Postdoctoral Science Foundation (2019M653316), the Chongqing Postdoctoral Science Foundation (cstc2019jcyj-bshX0017), the Fundamental Research Funds for the Central Universities (XDJK2019C017), the Open Project Program of the Laboratory of Chongqing Groundwater Resource Utilization and Environmental Protection (2019KZ00774), the Open Project Program of the Chongqing Key Laboratory of Karst Environment (Grant No. Cqk201801), and the Open Project Program of Guangxi Key Science and Technology Innovation Base on Karst Dynamics (KDL&Guangxi 202009).

References

Abbott, M.B., Bathurst, J.C., Cunge, J.A., O'Connell, P.E., Rasmussen, J., 1986a. An Introduction to the European HydrologicSystem-System Hydrologue Europeen, 'SHE', a: history and philosophy of a physically-based, distributed modelling system. J. Hydrol. 87, 45–59.

Abbott, M.B., Bathurst, J.C., Cunge, J.A., O'Connell, P.E., Rasmussen, J., 1986b. An Introduction to the European Hydrologic System-System Hydrologue Europeen, 'SHE', b: structure of a physically based, distributed modeling System. J. Hydrol. 87, 61–77.

Ambroise, B., Beven, K., Freer, J., 1996. Toward a generalization of the TOPMODEL concepts: topographic indices of hydrologic similarity. Water Resour. Res. 32, 2135–2145.

Baffaut, C., Benson, V.W., 2009. Modeling flow and pollutant transport in a karst watershed with SWAT. Trans. ASABE 52 (2), 469–479.

Bao, H.J., Wang, L.L., Li, Z.J., Yao, C., 2016. A distributed hydrological model based on Holtan runoff generation theory. J. Hohai Univ. (Natural Sci.) 4 (44), 340–346.

Bartolomé, A., Goldscheider, N., Vadillo, I., Jesús, M.V., Neukum, C., Sinreich, M., 2006. Karst groundwater protection: first application of a pan-european approach to vulnerability, hazard and risk mapping in the sierra de líbar (southern spain). Sci. Total Environ. 357 (1–3), 54–73.

Beven, K.J., Fisher, J.I., 1996. Remote sensing and scaling in hydrology. In: Stewart, J.B. (Ed.), Scaling Issues in Hydrology. Wiley, Chichester.

Birk, S., Geyer, T., Liedl, R., Sauter, M., 2005. Process-based interpretation of tracer tests in carbonate aquifers. Ground Water 43 (3), 381–388.

Bonacci, O., 2014. Hazards caused by natural and anthropogenic changes of catchment area in karst. Nat. Hazards Earth Syst. Sci. 4 (5/6), 655–661.

Chen, Y.B., 2009. Liuxihe Model. China Science and Technology Press, Beijing, China.

Chen, Y., 2018. In: Distributed Hydrological Models. Springer, Berlin Heidelberg, Berlin, Germany. https://doi.org/10.1007/978-3-642-40457-3_23-1.

Chen, Y., Li, J., Xu, H., 2016. Improving flood forecasting capability of physically based distributed hydrological models by parameter optimization. Hydrol. Earth Syst. Sci. 20, 375–392. https://doi.org/10.5194/hess-20-375-2016.

Chen, Y., Li, J., Wang, H., Qin, J., Dong, L., 2017. Large watershed flood forecasting with high-resolution distributed hydrological model. Hydrol. Earth Syst. Sci. 21 (735–749), 2017. https://doi.org/10.5194/hess-21-735-2017.

Chen, Y.F., Liao, Z., Zhou, J.Q., Hu, R., Yang, X.L., 2020. Non-darcian flow effect on discharge into a tunnel in karst aquifers. Int. J. Rock Mech. Min. Sci. 130, 104319.

Choi, J., Harvey, J. W., Conklin, M. H., 1999. Use of multi-parameter sensitivity analysis to determine relative importance of factors influencing natural attenuation of mining contaminants. the Toxic Substances Hydrology Program Meeting, Charleston,South Carolina.

Doummar, J., Sauter, M., Geyer, T., 2012. Simulation of flow processes in a large scale karst system with an integrated catchment model (MIKE SHE) – identification of relevant parameters influencing spring discharge. J. Hydrol. 426–427 (none), 112–123.

Fiorillo, F., Pagnozzi, M., Ventafridda, G., 2015. A model to simulate recharge processes of karst massifs. Hydrol. Process. 29 (10), 2301–2314.

Ford, D. C., Williams, P. W., 2007. Karst geomorphology and hydrology. Wiley, Chichester, England.

Freeze, R.A., Harlan, R.L., 1969. Blueprint for a physically based, digitally simulated, hydrologic response model. J. Hydrol. 9, 237–258.

Gallegos, J.J., Hu, B.X., Davis, H., 2013. Simulating flow in karst aquifers at laboratory and sub-regional scales using MODFLOW-CFP. Hydrogeol. J. 21 (8), 1749–1760.

Goldscheider, N., Drew, D., 2007. In: Methods in Karst Hydrogeology: IAH: International Contributions to Hydrogeology. CRC Press, pp. 26. https://doi.org/10.1201/9781482266023.

Hartmann, A., Goldscheider, N., Wagener, T., Lange, J., Weiler, M., 2014. Karst water resources in a changing world. review of hydrological modeling approaches. Rev. Geophys. 52 (3), 218–242.

Hartmann, A., Mudarra, M., Marín, A., Andreo, B., Wagener, T., 2015. Relating Land surface information and model parameters for a karst system in Southern Spain. Hydrogeological and environmental investigations in Karst Systems. Environ. Earth Sci., Springer, Berlin, Heidelberg. 1, 345–352.

Iacobellis, V., Castorani, A., Di Santo, A.R., Gioia, A., 2015. Rationale for flood prediction in karst endorheic areas. J. Arid Environ. 112, 98–108.

Kraller, G., Warscher, M., Strasser, U., Kunstmann, H., Franz, H., 2014. In: Distributed Hydrological Modeling and Model Adaption in High Alpine Karst at Regional Scale (Berchtesgaden Alps, Germany). Springer International Publishing, Switzerland. https://doi.org/10.1007/978-3-319-06139-9_8.

Li, J., Jiao, S.L., Liang, H., Xiang, Z., Xiang, S., 2012. Research on the impact on runoff by time-scale of the precipitation in karst basin in view of MIKE SHE model:a case in liudong river of the hongshuihe system. Carsologica Sin.

Li, J., Chen, Y., Wang, H., Qin, J., Li, J., Chiao, S., 2017. Extending flood forecasting lead time in a large watershed by coupling WRF QPF with a distributed hydrological model. Hydrol. Earth Syst. Sci. 21, 1279–1294. https://doi.org/10.5194/hess-21-1279-2017.

Li, J., Yuan, D., Liu, J., Jiang, Y., Chen, Y., Hsu, K.L., Sorooshian, S., 2019a. Predicting floods in a large karst river basin by coupling PERSIANN-CCS QPEs with a physically based distributed hydrological model. Hydrol. Earth Syst. Sci. 23 (1505–1532), 2019. https://doi.org/10.5194/hess-23-1505-2019.

Li, J., Hong, A., Yuan, D., Jiang, Y., Deng, S., Cao, C., Liu, J., Chen, Y., 2019b. Comparing the performances of WRF QPF and PERSIANN-CCS QPEs in karst flood simulations and forecasting with a new Karst-Liuxihe model. Hydrol. Earth Syst. Sci. Discussions. 1–48. https://doi.org/10.5194/hess-2019-285.

Linbin, C., Chihhao, T., Shihchang, L., Fuhsun, W.U., Chiwen, Y.U., 2010. Assessment of water inflow in mountain tunnel and back analysis for tunneling construction. Tunnel Constr. 30, 30–34.

Liu, J., Shen, L., Wang, Z., Duan, S., Wu, W., Peng, X., Jiang, Y., 2019. Response of plants water uptake patterns to tunnels excavation based on stable isotopes in a karst trough valley. J. Hydrol. 571, 485–493.

Lv, Y.X., Jiang, Y.J., Hu, W., Cao, M., Mao, Y., 2020. A review of the effects of tunnel excavation on the hydrology, ecology, and environment in karst areas: current status, challenges, and perspectives. J. Hydrol. 586, 1–15.

Meseguer, A., Mellibovsky, F., 2007. On a solenoidal fourier-chebyshev spectral method for stability analysis of the hagen-poiseuille flow. Appl. Numer. Math. 57 (8), 920–938.

Milanovic, P., 2002. The environmental impacts of human activities and engineering constructions in karst regions. Episodes 25 (1), 13–21.

Neukomm, M., Mercier, M., Jeannin, P.Y., Malard, A., Weber, E., 2020. Adapting tunnel construction to hydrogeological conditions in a karst region. Tunnels and Underground Cities: Engineering and Innovation meet Archaeology, Architecture and Art. DOI:10.1201/9780429424441-108.

Pan, H.Y., 2014. Hydrological model and application in karst watersheds. China University of Geosciences. Doctoral Dissertation, Wuhan, China.

Parise, M., Closson, D., Gutiérrez, F., Stevanović, Z., 2015. Anticipating and managing engineering problems in the complex karst environment. Environ. Earth Sci. 74 (12), 7823–7835.

Peterson, J.R., Hamlett, J.M., 1998. Hydrologic calibration of the SWAT model in a watershed containing fragipan soils. JAWRA J. Am. Water Resour. Assoc. https://doi.org/10.1111/j.1752-1688.1998.tb00952.x.

Qin, J.G., Jiang, Y.P., 2014. A review of numerical simulation methods for CFP pipeline flow. Groundwater 3, 98–100.

Raposo, J.R., Molinero, J., Dafonte, J., 2010. Quantitative evaluation of hydrogeological impact produced by tunnel construction using water balance models. Eng. Geol. 116 (3–4), 323–332.

Reimann, T., Melissa, E., Hill, 2009. Modflow-cfp: a new conduit flow process for modflow–2005. Ground Water. https://doi.org/10.1111/j.1745-6584.2009.00561.x.

ARTICLE IN PRESS

Ren, Q.W., 2016. Water Quantity Evaluation Methodology Based on Modified SWAT Hydrological Modeling in Southwest Karst Area. China University of Geoscience, Wuhan, China.

Schiller, A., Renard, P., 2016. An optical laser device for mapping 3D geometry of underwater karst structures. Boletin Geológico Y Minero. 127 (1), 99–110.

Suo, L.T., Wan, J.W., Lu, X.W., 2007. Improvement and application of TOPMODEL in karst region. Carsol. Sin. 26 (1), 67–70.

Valiantzas, J.D., 2008. Explicit Power Formula for the Darcy-Weisbach pipe flow equation: application in optimal pipeline design. J. Irrigation Drainage Eng.-ASCE 134 (4), 454–461.

Vigna, B., D'Angeli, I.M., De Waele, J., 2017. Hydrogeological flow in gypsum karst areas: some examples from northern Italy and main circulation models. Int. J. Speleol. 46 (2), 205. https://doi.org/10.5038/1827-806X.46.2.2095.

Vincenzi, V., Gargini, A., Goldscheider, N., 2009. Using tracer tests and hydrological observations to evaluate effects of tunnel drainage on groundwater and surface waters in the Northern Apennines (Italy). Hydrogeol. J. 17 (1), 135–150.

Wang, X., Li, S., Xu, Z., Hu, J., Pan, D., Xue, Y., 2019. Risk assessment of water inrush in karst tunnels excavation based on normal cloud model. Bull. Eng. Geol. Environ. 78 (5), 3783–3798.

Wu, W., Jiang, Y.J., Jia, Y.N., Peng, X.Y., Duan, S.H., Liu, J.C., 2018. Temporal and spatial distribution of the soil water δ D and δ18O in a typical karst valley: a case study of the Zhongliang mountain, Chongqing city. Environ. Sci. 39 (12), 5418–5427.

Xu, C., Xu, X., Liu, M., Li, Z., Zhang, Y., Zhu, J., 2020. An improved optimization scheme for representing hillslopes and depressions in karst hydrology. Water Resour. Res. 56. https://doi.org/10.1029/2019WR026038.

Yuan, D.X., 2002. China Karst Power Systems. Geological Publishing House, Beijing, China.

Zhang, Z.C., Chen, X., Shi, P., Wei, L.N., 2009. Distributed hydrological model and eco-hydrological effect of vegetation in Karst watershed. Adv. Water Sci. 20 (6), 54–59.

Zini, L., Chiara, C., Franco, C., 2015. The challenge of tunneling through Mediterranean karst aquifers: the case study of Trieste (Italy). Environ. Earth Sci. 74 (1), 281–295.